

Electrochemomechanical Energy Conversion in Nanofluidic Channels

Hirofumi Daiguji,^{*,†} Peidong Yang,^{‡,§} Andrew J. Szeri,^{||} and Arun Majumdar^{§,||}

Institute of Environmental Studies, Graduate School of Frontier Sciences, The University of Tokyo, Tokyo 113-0033, Japan, Department of Chemistry and Department of Mechanical Engineering, University of California, Berkeley, California 94720, and Materials Science Division, Lawrence Berkeley National Laboratory, Berkeley, California 94720

Received June 29, 2004; Revised Manuscript Received October 6, 2004

ABSTRACT

When the Debye length is on the order of or larger than the height of a nanofluidic channel containing surface charge, a unipolar solution of counterions is generated to maintain electrical neutrality. A pressure-gradient-driven flow under such conditions can be used for ion separation, which forms the basis for electrochemomechanical energy conversion. The current–potential ($I-\phi$) characteristics of such a battery were calculated using continuum dynamics. When the bulk concentration is large and the channel does not become a unipolar solution of counterions, both the current and potential become small. On the other hand, when bulk concentration is so much smaller, the mass diffusion becomes the rate-controlling step and the potential drops rapidly in the high current density region. When the Debye length of the solution is about half of the channel height, the efficiency is maximized.

Introduction. It is well known that when an external pressure gradient generates flow of an aqueous solution in a channel that contains a surface charge on its walls, a streaming current and a potential are produced.¹ This phenomenon depends critically on the surface charge and potential. In membrane science, the ζ -potential of a surface is an important and reliable indicator of the surface charge, and its knowledge is essential for design and operation of membrane processes. The streaming potential measurement is the most widely used technique for determining the ζ -potential of membranes, and it is performed in two different ways: (i) by flow through the membrane pore (transmembrane streaming potential)^{2–4} or (ii) by flow across the top surface of the membrane (tangential streaming potential).^{5–8}

Recently, Yang et al.⁹ proposed the concept of a battery using streaming current and streaming potential and reported results of a theoretical model and related experiments. They used a porous glass filter, 20 mm in diameter with pore sizes from 10 to 16 μm , and obtained a current of 1–2 μA from a 30 cm hydrostatic pressure drop. The maximum efficiency was estimated to be on the order of 0.01%. Because the streaming current is generated within the electrical double layer, the phenomenon is confined to within the Debye length, l_D , which characterizes the size of the layer. The

Debye length varies with salt concentration, n , as $l_D \propto n^{-1/2}$.¹⁰ Hence, for monovalent ions in the 0.1 M to 0.1 μM concentration range, l_D varies from 1 to 1000 nm, respectively. The remaining cross-sectional area of a microchannel does not contribute to net ionic transport. One way to utilize a larger fraction of the cross-sectional area and thereby improve battery performance is to reduce the channel height to nanometer scales. However, this would also increase viscous losses due to a higher surface-to-volume ratio of the channel. The purpose of this paper is to study mechanical-to-electrochemical energy conversion at nanometer scales and evaluate the performance characteristics.

Recently, Fan et al.¹¹ reported the synthesis of arrays of silica nanotubes with internal diameters in the range of 5–100 nm and with lengths 1–20 μm . Based on this, we proposed a unipolar ionic field-effect transistor as an application of these nanotubes.¹² The theoretical modeling of ionic distribution and transport in silica nanotubes, 30 nm in diameter and 5 μm long, suggested that when the diameter is smaller than the Debye length, a unipolar solution of counterions is created within the nanotube and the coions are electrostatically repelled. However, the effect of an external pressure gradient was not studied. The purpose of the present study is to investigate the transport phenomena inside nanotubes by means of an external pressure gradient and the resulting current–potential ($I-\phi$) characteristics of such a battery.

Governing Equations. The ion transport in nanofluidic channels due to diffusion and advection is analyzed using

* Corresponding author. E-mail: daiguji@k.u-tokyo.ac.jp, Tel: +81-3-5841-8587, Fax: +81-3-3818-0835.

† The University of Tokyo.

‡ Department of Chemistry, UC, Berkeley.

§ Lawrence Berkeley National Laboratory.

|| Department of Mechanical Engineering, UC, Berkeley.

continuum dynamics. The continuum dynamics equations assume that the transport coefficients are independent of position and time and that the state variables such as temperature and density do not vary appreciably in the system. The transport coefficients of diffusivity and viscosity are derived from molecular transport, that is, the diffusion of ions is due to the random walk of ions in liquid and the viscosity of liquid is due to the hopping of liquid molecules over the energy barrier between them. Since the energy barrier for molecular hopping depends on the intermolecular forces, the characteristic length and time scales depend on the changes in intermolecular forces in close proximity to a solid surface. These changes can be attributed to steric interactions ($\sim 1\text{--}2$ nm in range), electrostatic interactions (Debye length $\sim 1\text{--}100$ nm), and van der Waals interactions ($\sim 1\text{--}50$ nm). Except for steric interactions, other intermolecular forces can be modeled by continuum dynamics, which suggests that as long as the length scales are larger than 5 nm, continuum dynamics is an adequate description of liquid transport. Travis et al.¹³ reported that the velocity profiles are no longer quadratic at channel widths less than 10 molecular diameters in planar Poiseuille flow simulations of simple fluids. The channel height considered here is on the order of 10 nm, which is much larger than the length scale of molecular transport. Also, because the ion transport inside the Stern layer is neglected in our model,¹² the transport coefficients can be assumed to be independent of position and time. Furthermore, the hopping time scales can be written as $\tau \approx \nu^{-1} \exp(\Delta E/kT)$, where $\nu^{-1} \approx 10^{-13}$ s is the typical vibrational period and $\Delta E \leq 10kT$ is the typical energy barrier. Hence, the hopping time scale is $\tau \leq 10^{-9}$ s. Therefore, as long as the time scale of the phenomena under investigation is much longer than τ , continuum dynamics should be a reasonable assumption.

In the analysis of microchannel flow, the Poisson–Boltzmann equation is often assumed for the potential of an electrical double layer.^{14–16} This is valid when the electrical double layers of two adjacent walls do not overlap. For overlapping double layers, the Poisson–Nernst–Planck (PNP) equations^{17,18} and the Navier–Stokes (NS) equations are used to calculate the ionic current in nanofluidic channels. Yang et al.¹⁹ solved the PNP equations and the NS equations simultaneously without such assumptions in the analysis of microchannel flow. The potential at channel walls was given with the Dirichlet boundary condition, and the value was variable along the channel direction. But in this study, the Neumann boundary condition is employed and the gradient is determined by the surface charge density. In the Dirichlet boundary condition, the potential at channel walls is determined by considering not only the surface charge density but also the dimension of the channel, but in the Neumann boundary condition only the surface charge density is assumed, that is, the boundary condition is based on fewer assumptions. The governing equations are as follows:

$$\nabla^2 \phi = -\frac{1}{\epsilon_0 \epsilon} \sum_a z_a e n_a \quad (1)$$

$$\nabla(n_a \mathbf{u} + \mathbf{J}_a) = 0 \quad (2)$$

$$\nabla \mathbf{u} = 0 \quad (3)$$

$$\mathbf{u} \cdot \nabla \mathbf{u} = \frac{1}{\rho} \{-\nabla p + \mu \nabla^2 \mathbf{u} - (\sum_a z_a e n_a) \nabla \phi\} \quad (4)$$

The electrostatic potential ϕ is calculated with the Poisson equation (eq 1), where ϵ_0 is the permittivity of vacuum, ϵ is the dielectric constant of medium, n_a is the concentration of ions of species a , and $z_a e$ is their charge. The Nernst–Planck equation for ion species a can be written as eq 2, where \mathbf{J}_a is the particle flux due to concentration gradient and electric potential gradient, which is given by

$$\mathbf{J}_a = -D_a \left(\nabla n_a + \frac{(z_a e) n_a}{kT} \nabla \phi \right) \quad (5)$$

where D_a is the diffusivity of ion species a . The equation of continuity and the modified Navier–Stokes equations including electrokinetic effects can be written as eqs 3 and 4, respectively, where ρ is the fluid density and μ is the viscosity. The boundary conditions at channel walls are as follows:

$$\nabla_{\perp} \phi = -\frac{\sigma}{\epsilon_0 \epsilon} \quad (6)$$

$$\mathbf{J}_{a\perp} = 0 \quad (7)$$

$$\nabla_{\perp} p = \mu \nabla_{\perp}^2 u - \left(\sum_a z_a e n_a \right) \nabla_{\perp} \phi \quad (8)$$

$$\mathbf{u} = 0 \quad (9)$$

where \perp denotes the wall-normal component. The boundary condition for the Poisson equation is given by eq 6, where σ is the surface charge density. Here we assume that inside the Stern layer, the ions are rigidly held and do not contribute to the ionic current. If so, we do not need to calculate inside the Stern layer. The wall can be regarded as the interface between the Stern layer and the diffuse layer, and the surface charge density here is that of the wall plus that of ions within the Stern layer.^{1,10,20} The boundary condition for the flux equation is zero current through the wall (eq 7). The boundary condition for pressure is given by eq 8, and the velocity at the boundary is assumed to be zero (eq 9). These eqs 1–4 are solved simultaneously using a finite difference algorithm, yielding the electric potential, ionic densities, pressure, and velocity in the system.²¹ If these are known, the current density of the ion species a is obtained by the following equation:

$$\mathbf{i}_a = \mathbf{i}_{a,\text{adv}} + \mathbf{i}_{a,\text{dif}} = z_a e (n_a \mathbf{u} + \mathbf{J}_a) \quad (10)$$

The current through the channel is calculated by integrating the current density over the cross section,

$$\mathbf{I}_a = \int \mathbf{i}_a dS \quad (11)$$

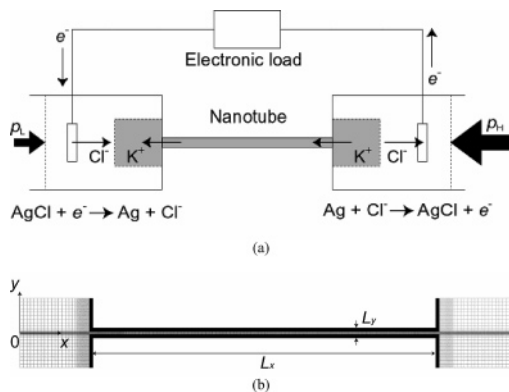


Figure 1. Electrochemomechanical battery. (a) Schematic diagram; (b) calculation system and computational grid (252×45) inside a silica nanotube with height of 30 nm, length of $5 \mu\text{m}$ with $1 \mu\text{m} \times 1 \mu\text{m}$ reservoirs on either side.

where S is the cross-sectional area of the channel. The dielectric constant of KCl aqueous solution, ϵ , is 80, the diffusivities of K^+ and Cl^- , D_{K^+} and D_{Cl^-} , are 1.96×10^{-9} and $2.03 \times 10^{-9} \text{ m}^2/\text{s}$, respectively.²² The density and viscosity of the solution are assumed to be 10^3 kg/m^3 and $10^{-3} \text{ Pa}\cdot\text{s}$, respectively.

Calculation System. Figure 1a and 1b show the schematic diagram of the whole system and the 2D domain for the calculation, where the total length of the channel, L_x , is $5 \mu\text{m}$ and the height, L_y , is 30 nm. Reservoirs $1 \mu\text{m} \times 1 \mu\text{m}$ in size are considered on either side of the channel. The surface charge density inside the channel ranged from 0 to $-5 \times 10^{-3} \text{ C/m}^2$. There are two calculation modes: the calculations of (i) the electromotive force, that is, the potential at zero current; and (ii) the current–potential characteristics, that is, the current at fixed potential biases. At the end of the reservoirs, the boundary conditions are given as follows:

$$\nabla\phi = 0 \text{ or } \phi = \phi_0, n_{\text{K}^+} = n_{\text{Cl}^-} = n_0, p = p_0, \nabla\mathbf{u} = 0 \quad (12)$$

In these boundary conditions, the electric potential is variable but the ionic densities adopt the bulk values. If the counterions transport through the channel and a streaming current is generated, the counterions are accumulated in one side of the reservoirs and this imbalance of charge generates the streaming potential. In this model, the chemical reactions at the electrodes and the external electric circuit are not considered explicitly, but these boundary conditions imply that the imbalance of charge instantly induces the chemical reactions at the electrodes in order to keep the solution in the reservoirs electrically neutral. The polarization at electrodes is completely neglected. Furthermore, the streaming current and the streaming potential are controlled by an electronic load (see Figure 1a). The boundary conditions of the walls face the reservoirs are as follows:

$$\nabla\phi = 0, \nabla n_{\text{K}^+} = \nabla n_{\text{Cl}^-} = 0, \nabla p = 0, \mathbf{u} = 0 \quad (13)$$

The boundary conditions at the inside walls of the channel are given by eqs 6–9. The grid spacing (see Figure 1b)

outside the channel is 50 nm, whereas the minimum grid spacing of 10 nm is assumed in the x direction near the inlets and outlets of the channel. The minimum grid spacing in the y direction is inside the channel and the value is 2 nm. Temperature is 300 K and the bulk concentration of KCl aqueous solution varies from 10^{-5} to 10^{-2} M .

Calculation Results. Calibration of Code. The 2D PNP code and the 2D Navier–Stokes equations were calibrated separately. The calibration method of the 2D PNP code was mentioned in ref 12. To calibrate the accuracy of the 2D Navier–Stokes equations code, the velocities in the x direction at $x = 3.5 \mu\text{m}$, were verified. When there is no electric field, the flow at $x = 3.5 \mu\text{m}$ is well developed and Poiseuille in nature. The velocity in the x direction is given by the following equation:

$$u(y) = -\frac{1}{2\mu} \frac{\partial p}{\partial x} \left\{ \left(\frac{L_y}{2} \right)^2 - y^2 \right\} \quad (14)$$

The velocities, $u(0)$, at $\partial p/\partial x = -10^{11} \text{ Pa/m}$ calculated with eq 14 and the calculation code are -0.01125 and -0.01124 m/s , respectively, which indicate excellent agreement.

Electromotive Force. Consider the concentration of KCl aqueous solution to be 10^{-4} M and the surface charge densities are -2.5×10^{-4} , -10^{-3} , and $-2 \times 10^{-3} \text{ C/m}^2$. The pressures at left and right reservoirs are 0 and $5 \times 10^5 \text{ Pa}$, respectively. Figure 2a shows the pressure and electric potential profiles at $y = 0$ and the ionic density profiles averaged over the y direction, along the x direction. Inside the channel the difference in concentration between K^+ and Cl^- is determined by the surface charge density. From the requirement of overall electroneutrality, the following equation is satisfied:

$$\Delta n = -\frac{2\sigma}{eL_y} \quad (15)$$

where Δn is the average concentration difference between K^+ and Cl^- in the y direction. When the surface charge densities are -2.5×10^{-4} , -10^{-3} , and $-2 \times 10^{-3} \text{ C/m}^2$ and the height of the channel is 30 nm, the difference $\Delta n = 1.04 \times 10^{23}$, 4.17×10^{23} , and $8.33 \times 10^{23} \text{ m}^{-3}$, which correspond to 0.17, 0.69, and 1.38 mM, respectively. The average concentration differences shown in Figure 2a (bottom) agree well with these values. If the bulk concentration is less than Δn , there exists a large potential barrier for the Cl^- ions to enter the channel, and the channel becomes essentially a “unipolar” solution of K^+ ions that neutralize the negative surface charge. By applying the pressure bias between two ends of a channel, the pressure driven flow is generated and the electric field is also generated to satisfy the zero current condition as shown in Figure 2a (middle). The electromotive forces calculated here are 0.30, 0.42, and 0.40 V, respectively. Figure 2b shows the pressure, potential, and concentration profiles in the y direction at $x = 3.5 \mu\text{m}$. When the surface charge density is small, these are distributed uniformly in the y direction. But as the surface charge density increases, the gradients increase and the distributions in the y direction cannot be neglected.

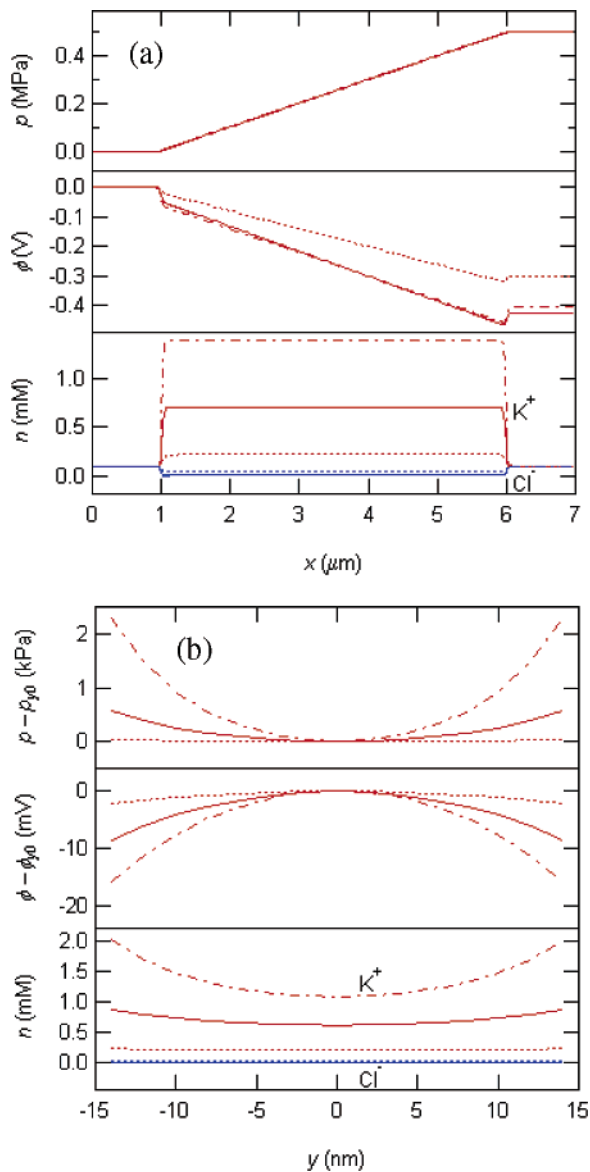


Figure 2. (a) Pressure (top) and electric potential (middle) profiles along the axis of symmetry, and concentration profiles in the x direction (bottom). (b) Pressure (top), electric potential (middle), and concentration (bottom) profiles in the y direction at $x = 3.5 \mu\text{m}$. The bulk concentration of KCl aqueous solution and pressure bias between two ends of the channel are assumed to be 10^{-4} M and 0.5 MPa, respectively. The surface charge densities are -2.5×10^{-4} (dotted lines), -10^{-3} (solid lines), $-2 \times 10^{-3} \text{ C/m}^2$ (broken lines).

Figures 3a and 3b show plots of the velocity vector and the local current density vector at $\sigma = -10^{-3} \text{ C/m}^2$, respectively. In this condition, the electrokinetic effects, that is, the third term in the right side of eq 4, are small and the velocity profile is almost the same to that of the Poiseuille flow expressed by eq 14. In Figure 3b, the current density vectors express the transport rates of counterions, because the concentration of coions inside the channel is almost zero. At zero current condition, the counterions circulate inside the channel and only water molecules pass through the channel from the right reservoir to the left one. To understand the distribution of current density vectors, one needs to carefully study the current density profiles in the y direction,

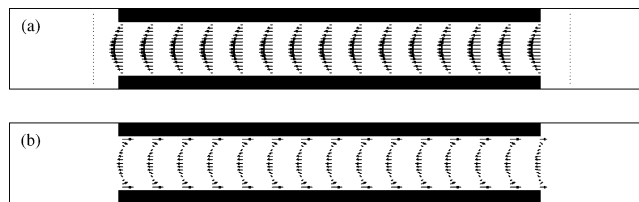


Figure 3. Plots of (a) velocity vectors and (b) current density vectors. The surface charge density on the tube surface and the bulk concentration of KCl aqueous solution are assumed to be -10^{-3} C/m^2 and 10^{-4} M, respectively. Pressure bias, $\Delta p = 0.5$ MPa is applied between the two ends of the nanotube.

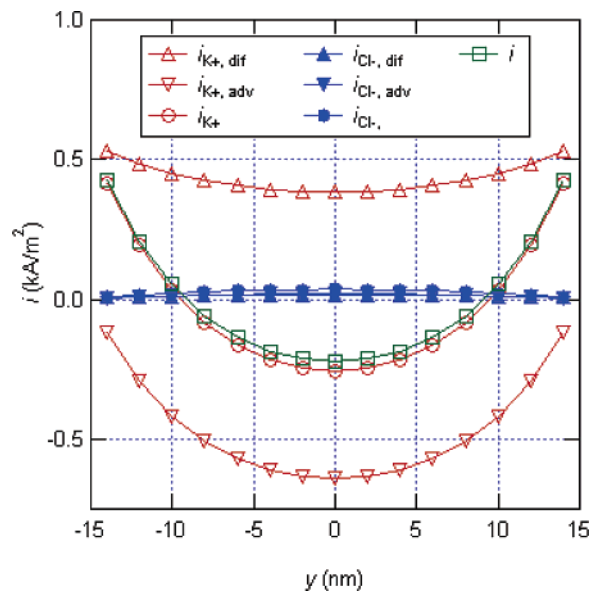


Figure 4. Current profiles in the y direction at $x = 3.5 \mu\text{m}$, for surface charge density, $\sigma = -10^{-3} \text{ C/m}^2$ on the channel surface. The bulk concentration of KCl aqueous solution and pressure bias are assumed to be 10^{-4} M and 0.5 MPa.

which are shown in Figure 4. The current density is a sum of two terms, the current densities due to advection and diffusion expressed by eq 10. For the current density of K^+ , the profile of current density due to advection is similar to the velocity profile and the direction is the flow direction. On the other hand the profile of current density due to diffusion is similar to the concentration profile and the direction is opposite to the flow direction. The superposition of these two profiles suggests that the direction of ionic current at the center of the channel is in the flow direction, whereas that near the wall is in the opposite direction. Hence, the K^+ ions circulate inside the channel without generating a net current.

Figure 5 shows the electromotive force as a function of the surface charge density of the channel for four different bulk concentrations of KCl aqueous solutions, 10^{-5} , 10^{-4} , 10^{-3} , and 10^{-2} M. The surface charge density ranges from 0 to $-5 \times 10^{-3} \text{ C/m}^2$. The pressure bias is 0.5 MPa. For the bulk concentrations, $n_0 = 10^{-5}$ and 10^{-4} M, when σ is larger than $-2 \times 10^{-3} \text{ C/m}^2$, the electromotive forces are almost the same but the discrepancy increases with decreasing σ . When the surface charge density is small, the average concentration difference between K^+ and Cl^- inside the channel, Δn , is not much larger than the bulk concentration

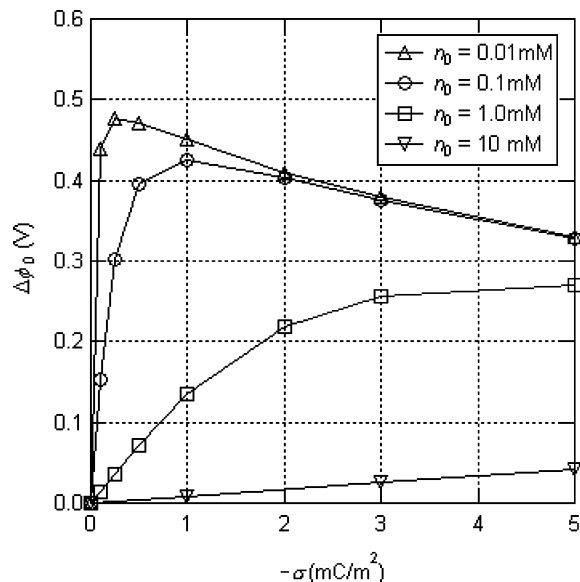


Figure 5. Electromotive force vs surface charge density ($\Delta\phi_0-\sigma$) curves. The bulk concentrations of KCl aqueous solutions are 10^{-5} , 10^{-4} , 10^{-3} , and 10^{-2} M. The pressure bias is 0.5 MPa.

at $n_0 = 10^{-4}$ M, the coions of Cl^- as well as the counterion of K^+ enter the channel. Hence, the solution inside the channel is not unipolar. As a result the electromotive force of $n_0 = 10^{-4}$ M is smaller than that of $n_0 = 10^{-5}$ M. As the surface charge density increases, only K^+ ions are located inside the channel independent of the bulk concentration, but they are accumulated near the channel walls (see Figure 2b, bottom). The K^+ ions near the walls do not contribute to the current density due to advection because the velocity near the wall is small. But the current density due to diffusion increases independent of its concentration profile. As a result the electromotive force decreases with increasing the surface charge density. There is an optimum surface charge density at which the maximum electromotive force can be generated. For the bulk concentration, $n_0 = 10^{-3}$ M, when the surface charge density is small, the unipolar solution of K^+ is not created inside the channel because the average concentration difference Δn is smaller than the bulk concentration n_0 . But as the surface charge density increases, Δn becomes larger than n_0 and the electromotive force increases. For the bulk concentration, $n_0 = 10^{-2}$ M, Δn is much smaller than n_0 in the whole range and the electromotive force is much smaller than those of other bulk concentrations.

Current–Potential Characteristics. To study the current–potential ($I-\Delta\phi$) characteristics, the bulk concentrations are assumed to be 10^{-5} , 10^{-4} , 10^{-3} , and 10^{-2} M and the pressure bias is assumed to be 0.5 MPa. Figure 6 shows the $I-\Delta\phi$ characteristics of these channels with the surface charge density of -10^{-3} and -5×10^{-3} C/m². Except for the $I-\Delta\phi$ characteristics of $n_0 = 10^{-5}$ M at $\sigma = -10^{-3}$ C/m² and $n_0 = 10^{-5}$ and 10^{-4} M at $\sigma = -5 \times 10^{-3}$ C/m², the curves are almost linear with negative gradient. This negative gradient expresses “ohmic drop”, i.e., the polarization that occurs when ionic current passes through the channel. When the average concentration difference between K^+ and Cl^- inside the channel, Δn , is much larger than the bulk concentration at n_0 , the mass diffusion becomes the rate-controlling step

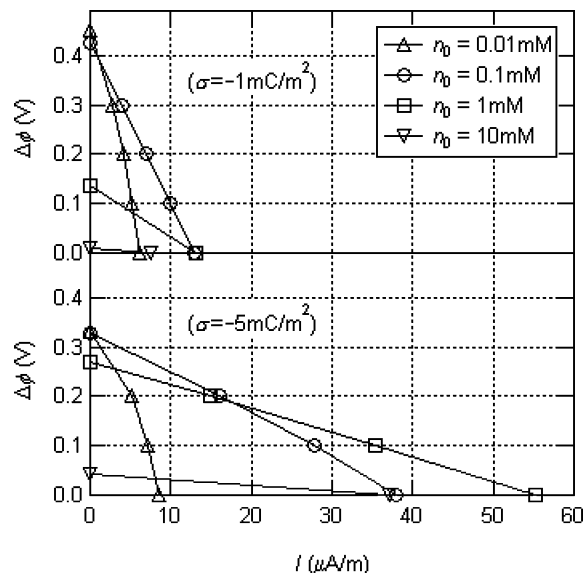


Figure 6. Current–potential ($I-\Delta\phi$) curves for two different surface charge densities, $\sigma = -10^{-3}$ C/m² (top) and $\sigma = -5 \times 10^{-3}$ C/m² (bottom) on the channel surface. The bulk concentrations of KCl aqueous solutions are assumed to be 10^{-5} , 10^{-4} , 10^{-3} , and 10^{-2} M. The pressure bias is 0.5 MPa.

and the potentials drop rapidly in the high current density region. When the surface charge density is -10^{-3} C/m², the calculated conductances for 10^{-4} , 10^{-3} , and 10^{-2} M KCl solutions are 30.5, 97.5, and 878.5 $\mu\text{S}/\text{m}$, respectively. When the surface charge density is -5×10^{-3} C/m², the conductances for 10^{-3} and 10^{-2} M KCl solutions are 204.7 and 913.4 $\mu\text{S}/\text{m}$, respectively. The conductance of the channel increases with increasing the bulk concentration as well as the surface charge density. But these two effects on the conductance are nonlinear.

Efficiency. The efficiency is one of the most important performance indicators for energy conversion systems. The input power, the output power, and the efficiency can be expressed as follows:

$$P_{\text{in}} = \Delta p \int_{-L_y/2}^{L_y/2} u(y) dy \quad (16)$$

$$P_{\text{out}} = \Delta\phi I \quad (17)$$

$$\eta = \frac{P_{\text{out}}}{P_{\text{in}}} \quad (18)$$

Assuming the Poiseuille flow, the input power is calculated to be 112.5 $\mu\text{W}/\text{m}$ at $L_x = 5 \mu\text{m}$, $L_y = 30 \text{ nm}$, and $\Delta p = 0.5$ MPa. But the volumetric flow rate slightly decreases with increasing the potential and decreasing the current. Here, the volumetric flow rate is assumed to be proportional to the potential and current for simplicity. If the $I-\Delta\phi$ characteristics are assumed to be linear, for the surface charge density $\sigma = -10^{-3}$ C/m², the maximum output power is 1.36 $\mu\text{W}/\text{m}$ and the maximum efficiency is 1.26% at $n_0 = 10^{-4}$ M (at $I = 6.40 \mu\text{A}/\text{m}$ and $\Delta\phi = 0.215$ V). For the surface charge density $\sigma = -5 \times 10^{-3}$ C/m², the maximum output power is 3.73 $\mu\text{W}/\text{m}$ and the maximum efficiency is 3.56% at n_0

$= 10^{-3}$ M (at $I = 26.7 \mu\text{A}/\text{m}$ and $\Delta\phi = 0.139$ V). When the bulk concentration n_0 is larger than the average concentration difference between K^+ and Cl^- , Δn , the channel does not become a unipolar solution of K^+ ions and the currents and potentials become small. On the other hand, when n_0 is so much smaller than Δn , the mass diffusion becomes the rate-controlling step and the potentials drop rapidly in the high current density region. As a result, when the electrical double layers overlap near the center of the channel, the Debye length of a solution is about half of the channel height, the efficiency is maximized.

Discussion. Two required conditions for the high performance battery are: (i) the channel becomes a unipolar solution of K^+ ions; and (ii) the mass diffusion is not the rate-controlling step. When these two conditions are satisfied, the electromotive force, $\Delta\phi_0$, and the current at zero potential, I_0 , can be expressed as follows:

$$\Delta\phi_0 = \frac{L_x}{-2\sigma} \frac{kT}{D_{\text{K}^+}} \int_{-L_y/2}^{L_y/2} n_{\text{K}^+}(y)u(y) dy \quad (19)$$

$$I_0 = e \int_{-L_y/2}^{L_y/2} n_{\text{K}^+}(y)u(y) dy \quad (20)$$

where n_{K^+} is the concentration of K^+ ions. When the ion distribution in the y direction is uniform, the integral, $\int_{-L_y/2}^{L_y/2} n_{\text{K}^+}(y)u(y) dy$ becomes maximum, $-2\sigma\bar{u}/e$, where $\bar{u} = \int_{-L_y/2}^{L_y/2} u(y) dy/L_y$. Furthermore, when the flow is well developed and Poiseuille in nature and the electrokinetic effects, the third term of in the right side of eq 4, are neglected, the average velocity, \bar{u} becomes maximum, $L_y^2\Delta p/12\mu L_x$, at a fixed axial gradient of pressure, $\Delta p/L_x$. In these conditions, eqs 19 and 20 become

$$\Delta\phi_0 = \frac{kT}{12D_{\text{K}^+}e\mu}(L_y^2\Delta p) \quad (21)$$

$$I_0 = \frac{1}{6\mu} \left(\frac{L_y^2\Delta p|\sigma|}{L_x} \right) \quad (22)$$

Assuming the current–potential ($I-\Delta\phi$) curve is linear and the maximum output power is calculated as $\Delta\phi_0 I_0/4$, the maximum output power and efficiency of the battery can be expressed as follows:

$$P_{\text{max}} = \frac{kT}{288D_{\text{K}^+}e\mu^2} \left(\frac{L_y^4\Delta p^2|\sigma|}{L_x} \right) \quad (23)$$

$$\eta_{\text{max}} = \frac{kT}{24D_{\text{K}^+}e\mu}(L_y|\sigma|) \quad (24)$$

At $L_x = 5 \mu\text{m}$, $L_y = 30 \text{ nm}$, and $\Delta p = 0.5 \text{ MPa}$, for the surface charge density $\sigma = -10^{-3} \text{ C}/\text{m}^2$, the calculation results of eqs 21–24 become $\Delta\phi_0 = 0.49 \text{ V}$, $I_0 = 15.0 \mu\text{A}/\text{m}$, $P_{\text{max}} = 1.86 \mu\text{W}/\text{m}$, and $\eta_{\text{max}} = 1.65\%$. These values are in reasonable agreement with the former calculated results at $n_0 = 10^{-4} \text{ M}$. For the surface charge density $\sigma = -5 \times$

$10^{-3} \text{ C}/\text{m}^2$, the corresponding results become $\Delta\phi_0 = 0.49 \text{ V}$, $I_0 = 75.0 \mu\text{A}/\text{m}$, $P_{\text{max}} = 9.28 \mu\text{W}/\text{m}$, and $\eta_{\text{max}} = 8.25\%$. These values are much larger than the former calculated results at any bulk concentration. In these conditions, the ion distribution in the y direction and the electrokinetic effects cannot be neglected and eqs 19 and 20 must be used in the calculation of $\Delta\phi_0$ and I_0 . But one may obtain an analytical solution for the electrical potential, ion concentration, velocity, and pressure fields. We address the calculation method in the Appendix. From eqs 23 and 24, the maximum output power, P_{max} , is proportional to L_x^{-1} , L_y^4 , ΔP^2 , and $|\sigma|$, and the maximum efficiency, η_{max} , is proportional to L_y and $|\sigma|$ and independent of L_x and ΔP . It is noted that for tubes with diameter of d instead of 2D channels with channel height of L_y , the maximum power varies as $P_{\text{max}} \propto d^5$ instead of $P_{\text{max}} \propto L_y^4$. In general, as L_y and $|\sigma|$ increase, the ion distribution becomes nonuniform and the maximum output power and efficiency become smaller than the values calculated with eqs 23 and 24. As they increase further, the two required conditions for the high performance battery cannot be satisfied at the same time and the maximum output power and efficiency are deteriorated. And as Δp increase and L_x decreases, the velocity of solution increases and the mass diffusion easily becomes the rate-controlling step.

Conclusions. The Poisson–Nernst–Planck equations and the Navier–Stokes equations were employed to calculate ionic distribution and transport by a pressure driven flow in a nanofluidic channel, $5 \mu\text{m}$ long and 30 nm high. The pressure bias was 0.5 MPa . The surface charge density ranged from 0 to $-5 \times 10^{-3} \text{ C}/\text{m}^2$, the bulk concentration of KCl aqueous solution ranged from 10^{-5} to 10^{-2} M .

The following conclusions can be drawn from this study. (1) When the channel size is smaller than the Debye length and the channel surface is charged, the channel becomes a unipolar solution of counterions at a concentration that neutralizes the surface charge. The coions are essentially repelled from the channel. (2) If the pressure bias is applied between two ends of the nanotube filled with a unipolar solution of counterions, only the counterions could pass through the nanotube and the streaming current and streaming potential are generated. This could form the basis for a battery. (3) At the zero current condition, the counterions are circulated inside the channel and only the water molecules pass through the channel. As the potential bias decreases, the counterions as well as the water molecules pass through the channel and the streaming current is generated. (4) The electromotive force is a function of the surface charge density and the bulk concentration. Two important factors that contribute to high electromotive force are that: (i) a unipolar solution of counterions is generated and (ii) the ions are distributed uniformly inside the channel. (5) For the efficiency of a battery, when the bulk concentration is large and the channel does not become a unipolar solution of counterions, both the current and potential become small. On the other hand, when bulk concentration is so much smaller, the mass diffusion becomes the rate-controlling step and the potential drops rapidly in the high current density region. When the Debye length of the solution is about half of the channel height, the efficiency is maximized.

Acknowledgment. This research was partially supported by the Japanese Ministry of Education, Culture, Sports, Science and Technology, Grant-in-Aid for Young Scientists (B), 16760149, 2004. This work was partially supported through a grant from Basic Energy Sciences, Department of Energy. A.M. would like to thank the Miller Institute for their support through a Miller Professorship.

Appendix

In a long channel, when the flow is fully developed, one may obtain an analytical solution for the electrical potential, ion concentration, velocity, and pressure fields as follows. The translation invariance of the boundary conditions and field equations suggest a search for solutions in which: the x -dependence is linear in ϕ and p , with additive y -dependence $\tilde{\phi}(y)$ and $\tilde{p}(y)$ and potassium ion concentration $n_{K^+}(x,y,z) = \tilde{n}_{K^+}(y)$ and velocity field $\mathbf{u}(x,y,z) = \{\tilde{\mathbf{u}}(y), 0, 0\}$. The equations are then solvable in closed form. The potassium ion concentration is $\tilde{n}_{K^+}(y) = C \exp[-e/kT \tilde{\phi}(y)]$, where C is a constant and the coion concentration is assumed to be zero. This may be substituted into Poisson's equation, which yields a nonlinear, two-point boundary value problem for the electrical potential, with solution $\tilde{\phi}(y) = -kT/e \log [\sec^2(\sqrt{e^2 C/2kT\epsilon_0\epsilon} y)]$. The channel wall boundary condition involving the surface charge evaluated then yields a transcendental equation for C :

$$\sqrt{C} \tan\left(\sqrt{\frac{e^2 C}{2kT\epsilon_0\epsilon}} \frac{L_y}{2}\right) = -\frac{\sigma}{\sqrt{2kT\epsilon_0\epsilon}} \quad (25)$$

The solution for the velocity field is

$$\tilde{\mathbf{u}}(y) = -\frac{1}{8\mu} \frac{\partial p}{\partial x} (L_y^2 - 4y^2) - \frac{2kT\epsilon_0\epsilon}{e\mu} \frac{\partial \phi}{\partial x} \log \left[\frac{\cos\left(\sqrt{\frac{e^2 C}{2kT\epsilon_0\epsilon}} y\right)}{\cos\left(\sqrt{\frac{e^2 C}{2kT\epsilon_0\epsilon}} \frac{L_y}{2}\right)} \right] \quad (26)$$

The solution for the pressure is $\tilde{p}(y) = kTC \tan^2$ -

$(\sqrt{e^2 C/2kT\epsilon_0\epsilon} y)$. Closed form expressions may likewise be obtained for the total current density in the flow direction $\tilde{i}_{K^+,x}(y)$ and its integral across the channel, $I_{K^+,x}$, but these are too long to repeat here. The input and output power per unit length of the channel are $P_{in} = \partial p/\partial x \int_{-L_y/2}^{L_y/2} \tilde{\mathbf{u}}(y) dy$, $P_{out} = \partial \phi/\partial x \int_{-L_y/2}^{L_y/2} \tilde{i}_{K^+,x}(y) dy$. Hence, to solve a problem, one must fix the axial gradients $\partial \phi/\partial x$ and $\partial p/\partial x$. For the surface charge density σ , eq 25 yields the constant C by trivial numerical solution. Then the fields and power input and output are as given in the preceding. Tested against the numerical solutions in the channel, the analytical solution shows excellent agreement.

References

- (1) Hunter, R. J. *Zeta Potential in Colloid Science*; Academic Press: London, 1981.
- (2) Nyström, M.; Lindström, M.; Matthiasson, E. *Colloids Surf.* **1989**, *36*, 297–312.
- (3) Kim, K. J.; Fane, A. G.; Nyström, M.; Pihlajamäki, A.; Bowen, W. R.; Mukhtar, H. *J. Membr. Sci.* **1996**, *116*, 149–159.
- (4) Szymczyk, A.; Pierre, A.; Reggiani, J. C.; Pagetti, J. J. *J. Membr. Sci.* **1997**, *134*, 59–66.
- (5) Van Wagenen, R. A.; Andrade, J. D. *J. Colloid Interface Sci.* **1980**, *76*, 305–314.
- (6) Möckel, D.; Staude, E.; Dal-Cin, M.; Darcovich, K.; Guiver, M. *J. Membr. Sci.* **1998**, *145*, 211–222.
- (7) Sbaï, M.; Szymczyk, A.; Fievet, P.; Sorin, A.; Vidonne, A.; Pellet-Rostaing, S.; Favre-Reguillon, A.; Lemaire, M. *Langmuir* **2003**, *19*, 8867–8871.
- (8) Fievet, P.; Sbaï, M.; Szymczyk, A.; Vidonne, A. *J. Membr. Sci.* **2003**, *226*, 227–236.
- (9) Yang, J.; Lu, F.; Kostiuk, L. W.; Kwok, D. Y. *J. Micromech. Microeng.* **2003**, *13*, 963–970.
- (10) Israelachvili, J. *Intermolecular and Surface Force*, 2nd ed.; Academic Press: London, 1992.
- (11) Fan, R.; Li, D.; Majumdar, A.; Yang, P. *J. Am. Chem. Soc.* **2003**, *125*, 5254–5255.
- (12) Daiguji, H.; Yang, P.; Majumdar, A. *Nano Lett.* **2004**, *4*, 137–142.
- (13) Travis, K. P.; Todd, B. D.; Evans, D. J. *Phys. Rev. E* **1997**, *55*, 4288–4295.
- (14) Gad-el-Hak, M. *The MEMS Handbook*; CRC Press: Boca Raton, FL, 2002.
- (15) Arulanandam, S.; Li D. *Colloids Surf. A* **2000**, *161*, 89–102.
- (16) Patankar, N. A.; Hu, H. H. *Anal. Chem.* **1998**, *70*, 1870–1881.
- (17) Eisenberg, R. S. *J. Membr. Biol.* **1996**, *150*, 1–25.
- (18) Eisenberg, R. S. *J. Membr. Biol.* **1999**, *171*, 1–24.
- (19) Yang, R.; Fu, L.; Hwang, C. *J. Colloid Interface Sci.* **2001**, *244*, 173–179.
- (20) Brett, C. M. A.; Brett, A. M. O. *Electrochemistry, principles, methods, and applications*; Oxford University Press: Oxford, 1993.
- (21) Kumikova, M. G.; Coalson, R. D.; Graf, P.; Nitzan, A. *Biophys. J.* **1999**, *76*, 642–656.
- (22) Hille, B. *Ion channels of excitable membrane*, 3rd ed.; Sinauer Associates Inc.: Sunderland, MA, 2001.

NL0489945